CHAPTER-V

Microstructural Transition of Water to Acetonitrile-Based Reverse Micelle through Binary Compositions of Polar Solvents

V.1. Introduction

Reverse micelles (RMs) are formed when amphiphilic molecules self-aggregate in a non-polar solvent. They are broadly classified into aqueous or non-aqueous RMs depending on the nature of co-solvents e.g., water or polar organic solvents, which control the chemistry occurring in them [1]. The geometric confinement inside RMs modifies the properties of entrapped polar solvent compared to that of bulk solvent. Even though water is traditionally the most common and versatile polar solvent, a variety of non-aqueous polar solvents were also used to create RMs due to certain distinct advantages, such as improved stability, large variety of tunability and to customize a water-free reaction medium [2]. Friberg and Podzimek first time studied non aqueous RMs using ethylene glycol [3]. Later on, Falcone et al. investigated the properties of non-aqueous RMs using large variety of polar solvents, viz., glycerol, ethylene glycol, propylene glycol, formamide, dimethylformamide and dimethylacetamide [4]. Recently, Correa et al. reviewed a detail discussion on RMs formed with polar solvents other than water both from the perspective of fundamental characterization and application for novel chemistry [1]. Several literatures have appeared in recent times which report the formation of RMs using acetonitrile (ACN) as well [5–10], but whether ACN molecules are effectively encapsulated by the surfactant molecules forming a true RMs, remains unclear. Almost all of these studies relied on the steady state absorption and emission spectroscopies including time-resolved spectroscopic technique to understand the effective encapsulation and the salvation dynamics of ACN in RMs. The difference between ACN-based RMs from aqueous or methanol-based RMs was interpreted on the basis of hydrogen bonding ability of water and ACN [5–10].

However, above studies, in general, provide information concerning the microenvironment and dynamics of the confined geometry; none of these reports explored the formation stability of RMs along with the droplet size and other microstructural characteristics. In order to understand the scientific basis for the microstructural modification between ACN-based non-aqueous RMs with that of aqueous RMs, we have formulated and characterized RMs in cyclohexane (Cy) using didodecyldimethylammonium bromide (D_{12}DAB) as the cationic surfactant, by solubilizing water and ACN at different binary compositions. While the double tailed anionic surfactant viz., sodium bis(2-ethylhexyl) sulfosuccinate (AOT) is one of the most thoroughly utilized for RMs, the double tailed cationic D_{12}DAB also can effectively form RMs in nonpolar solvents without a cosurfactant [11]. But surprisingly, it had received relatively less attention from the scientists working in this field. On the other hand, while much attention has been paid so far to the microenvironmental features of ACN-based RMs, relatively less is known about the microstructural properties of the RMs with entrapped ACN and/or water. To the best of our knowledge, no attempt has ever been made to study the microstructures and stability of RMs as a function of binary solvent mixture, water and ACN (v/v). The motivation of choosing different binary compositions of water and ACN for the entrapment in the RMs originates from the reported synergistic performance of polar solvent mixtures in comparison to the individual component, in which, addition of 38% v/v mixture of glycerol (GY) with water in AOT/n heptane RMs resulted in an increase in the catalytic properties of achymotrypsin (a-CT) during hydrolysis of 2-naphthyl acetate [12]. Binary mixtures of ACN and water are widely used as reaction media in diverse fields of physical-organic chemistry, reverse phase liquid chromatography, and electrochemistry, solvent extraction, and atmospheric chemistry [13]. In this report, conductivity and dynamic light scattering (DLS) measurements were employed to investigate the gradual changes occurring in the microstructure of the RMs on going from aqueous to non-aqueous RMs via several mixed compositions of water and ACN. The nature of various water and ACN states inside D_{12}DAB RMs has been studied by using Fourier transform infrared (FTIR) spectroscopy. Also, the microstructural transition between aqueous and non aqueous RMs, based on anionic AOT surfactant was carried out and compared in order to clarify the effect of surfactant charge types. The results which justify the conjecture of the existence of

polar non-aqueous nano-pool are presented and the thermal stability of formulated system is also discussed in terms of efficiency of H-bonding inside the droplet core.

V.2. Materials and methods

V.2.1 Materials

Didodecyldimethylammonium bromide, D_{12}DAB (98%, CAS Number 3282-73-3), sodium bis (2-ethylhexyl) sulfosuccinate, AOT (96%, CAS Number 577-11-7) and cyclohexane (≥ 99.9%, CAS Number 110-82-7) with best available analytical grade were purchased from Aldrich and Sigma-Aldrich, respectively and used without further purification. Ultrapure acetonitrile (ACN) (CAS No. 75-05-8, L010300 Sigma), deuterium oxide (99.9 atom% D, CAS Number 7789-20-0, Aldrich), methyl red (CAS No. 493-52-7, 250198 Sigma-Aldrich) and cobalt (II) chloride hexahydrate (CAS No. 7791-13-1, C8661 Sigma) were all of analytical grade. Double distilled water was used for all sample preparations with specific conductance of 2-4 μS cm^{-1}.

V.2.2 Preparation of reverse micellar solution

Stock solution of D_{12}DAB in cyclohexane was prepared by weight and volumetric dilution. Aliquots of this stock solution were used to prepare a series of reverse micellar systems by adding varied quantity of polar solvent [e.g., water or ACN, or binary mixture of water and ACN (v/v)]. Polar solvent was added by a calibrated microsyringe and the resultant mixtures were shaken in a sonication bath to obtain optically clear solutions exhibiting single phase. The obtained clear solutions correspond to aqueous or non-aqueous or water or ACN-rich reverse micelles (RMs) with polar solvent-to-surfactant molar ratio (R). In all cases, the D_{12}DAB surfactant concentration was kept constant at 0.3 M in cyclohexane.

V.2.3 Instruments and Methods

V.2.3.1 Electrical conductivity measurement: The electrical conductivity measurements were performed using Mettler Toledo (Switzerland) Conductivity Bridge. The instrument was calibrated with standard KCl solution. The temperature was kept constant (298 K) for conductivity measurement within ± 0.01 ^{0}C by circulating thermostated water bath, through a jacketed vessel containing the solution.

A fixed volume of surfactant-oil solution was taken at constant surfactant concentration in thermostated water bath. After that corresponding polar solvent was added gradually until the phase separation occurred and conductance was measured after each addition. The repeatability and the accuracy of the measurements were ± 0.3 and ± 1 %, respectively.

V.2.3.2 Dynamic light scattering (DLS) measurement: DLS measurements were carried out using a Zetasizer Nano ZS90 (ZEN3690, Malvern Instruments Ltd, U.K.). A He-Ne laser of 632.8 nm wavelength was used and the measurements were made at a scattering angle of 90^0 at experimental temperature. Temperature was controlled by inbuilt Peltier heating-cooling device (± 0.1 K). Refractive index of each solution was recorded with an ABBE type refractometer, as it was required as an input in determining the size of the RM droplet by DLS technique. Viscosity data, as obtained from viscosity measurements, were used in processing DLS data. Samples were filtered thrice using Milipore(TM) hydrophobic membrane filter of 0.25µ pore size. Hydrodynamic diameter (D_h) of the RM droplets was estimated according to Stokes-Einstein equation, which defined as;

$$D_h = k_B T / 3\pi\eta D \quad (1)$$

Where, k_B, T, η and D indicate the Boltzmann constant, temperature, viscosity and diffusion coefficient of the solution, respectively. To check the reproducibility of the results at least 6 measurements were done.

V.2.3.3 Fourier transform infrared spectroscopy (FTIR) measurements: FTIR absorption spectra were recorded in the wave number range of 400-4000 cm^{-1} with a Shimadzu 83000 spectrometer (Japan) using a CaF_2-IR crystal window (Sigma-Aldrich) equipped with Presslock holder with 100 number scans and spectral resolution of 4 cm^{-1} at 298 K. Deconvolution was carried out with the help of Origin 6.0 software.

V.2.3.4 Ultraviolet-visible spectroscopy (UV-Vis) measurements: UV/Vis electronic absorption spectra were recorded on a Jasco (V-530) spectrophotometer at 298 K. The path length of the quartz cell used in this experiment was 1 cm. The RM solutions were prepared in advance and then added to the quartz cell.

V.2.3.5 Quantum chemical calculations: Ab *initio* calculations were performed using the Gaussian09 (G09) program [51]. Geometry optimizations, and vibrational frequency analysis were performed at the level of Hartee Fock (HF) and using the 6-31G basis set. Various different initial configurations are considered, in which D_{12}DAB, AOT, ACN and water molecules were placed at different locations. Optimizations of these configurations were performed without any constraints in the geometry. The lowest energy structure among all the explored geometries was designated as the optimized structure. The optimized structures represented true minima since no imaginary frequency was observed in the harmonic frequency analysis. The basis set superposition errors (BSSEs) were corrected using the counterpoise method of Boys and Bernardi [52]. The vibrational FT-IR frequency calculations were performed on the geometry optimized structure of the molecules using Density Functional Theory (DFT) with the CAM-B3LYP/cc-pVDZ method in G09 [51].

V.3. Results and Discussion

V.3.1 Solubilization capacity of RMs as a function of binary compositions of polar solvent

In order to detect the structural transitions from aqueous D_{12}DAB/Cy RMs to ACN-based non aqueous system, the stability of formulated systems as a function of composition of binary polar solvents is determined; this is defined as the ratio of maximum solubilization limit of the corresponding polar solvent (above which phase separation takes place) in this report. For this purpose, we have used total eleven compositions of polar solvent (v/v) for entrapment in RMs, such as aqueous RMs (100% of water), non-aqueous RMs (100% of ACN) and RMs with binary compositions of ACN and water (10% to 90% of ACN, v/v). Fig 1 displays the variation of transparent RMs region (1f) as a function of binary compositions of entrapped ACN. The solubilization capacity (R) of RMs is expressed in terms of the ratio, R= [polarsolvent]/[surfactant], where molecular weights of both polar solvents were considered in order to calculate the molar concentrations of polar solvents at binary compositions. However, for 100% (v/v) water-based RM systems, the solubilization ability is expressed as the water/surfactant molar ratio (ω_0) of 3.70.

Interestingly, the D_{12}DAB RMs exhibit considerable synergism in the solubilization capacity of corresponding polar solvent (R) wherein R initially increases with increasing compositions of ACN (v/v) and passes through a maximum at 50% of ACN in mixed polar solvents, beyond which it decreases. Whereas, the synergistic solubilization capacity is observed at 20% of ACN in mixed polar solvents for AOT-RMs. Addition of ACN can expel part of the surfactant molecules from the aqueous phase to the organic phase to form RMs and hence solubilization increases. Also, ACN decreases the interaction among the droplets by making the interfacial layer more rigid, which in turn also increases solubilization. At a higher concentration of ACN, a different phenomenon overcomes this effect, where addition of ACN decreases the thickness of the electrical double layer of the charged interfacial film. Subsequently, the effective polar area of the surfactant also decreases. This in turn increases the tendency of the surfactant to form natural negative curvature, which decreases the solubilization [14,15]. It may also be noted that AOT is the least polar surfactant compared to D_{12}DAB (HLB values of D_{12}DAB and AOT are 18.1 and 10.2, respectively [16,17]), and the least [ACN] is required to bring about the solubilization maximum among the studied systems. This clearly indicates the direct influence of interfacial charge types of RMs during the formation. The observed phenomenon, related to maximum water solubilization capacity in RMs, is not uncommon in literature. However, such a synergism was reported earlier for AOT based RMs as a function of the content of the added second surfactant, co-surfactant, additive concentration (electrolyte or ionic liquid, IL) and chain length of the oil [14,18–20]. Both D_{12}DAB and AOT RMs showed similar synergism in water solubilization capacity but in presence of added ionic and non-ionic surfactants [21,22]. It would be now interesting to investigate whether such a modification imprints the microstructural characteristics of the encapsulated water and/or ACN molecules inside these RMs.

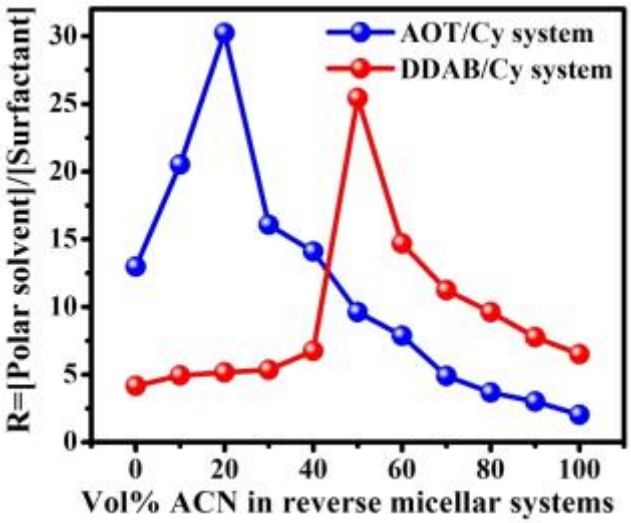

Figure 1. Variation of solubilization capacity of D_{12}DAB or AOT/cyclohexane reverse micelles (RMs) with increase in acetonitrile (ACN) content in mixed compositions of polar solvents (water or ACN, v/v) at 298 K. The red/blue dotted line indicates the experimental paths.

V.3.2 Size distribution of D_{12}DAB/Cy-based reverse micellar droplets by DLS technique

A series of samples from 1F region of RMs (Fig 1) were chosen at a fixed volume of polar solvent with different compositions of water/ACN (v/v) and measured by DLS, which proved to be a powerful tool for characterization of the size and size distribution of RM droplets. Fig 2A and 2B demonstrates the size distributions and individual droplet sizes of the chosen RM samples at 298 K. It is evident from the figures that pure aqueous RMs (100% water, v/v) produced larger droplets in comparison to non-aqueous one (100% ACN, v/v). Previously, Riter et al. noticed similar trend in droplet size of AOT/isooctane-RMs in presence of water and ACN [23]. The addition of ACN gives rise to a decrease in the repulsive interaction between the head groups of the ionic surfactant, D_{12}DAB, which further increases the packing parameter of surfactant molecules [24] (P= v/al, where 'v' and 'l' are the volume and the length of hydrophobic chain, respectively and 'a' is the area of polar head group of the surfactant) and decreases the droplet diameter. Also, the addition of ACN within the reverse micellar water pool weakens the hydrogen-bonding between water and head group of D_{12}DAB and thereby reduces hydration of cationic head group, i.e., decrease in 'a' and

subsequently increase in “P” value of surfactant. This results in the formation of smaller droplets due to decreasing their swelling [25].

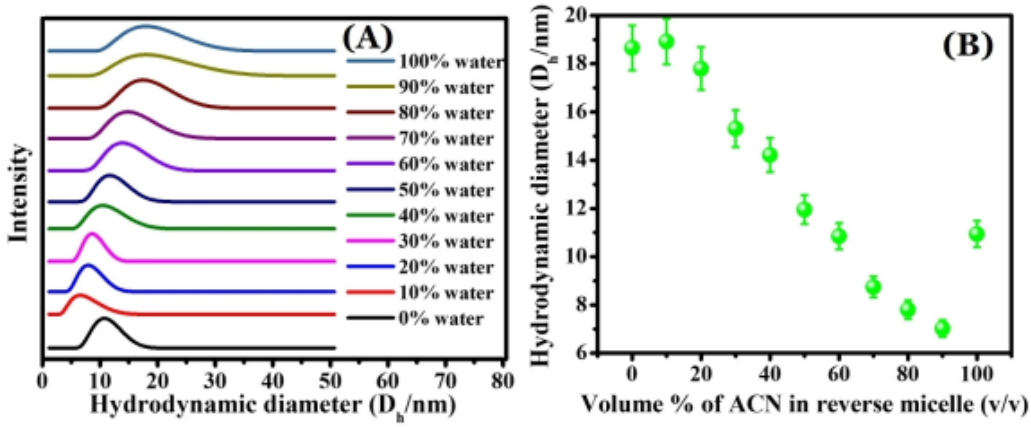

Figure 2. (A) Droplet size distribution, and (B) variation of droplet sizes of D_{12}DAB/cyclohexane reverse micelles (RMs) composed of different binary compositions of polar solvents (water or ACN, v/v) at 298 K. Herein, 10% water to 100% (v/v) water systems correspond to the water/surfactant molar ratio (ω_0) of 0.37 to 3.70.

V.3.3 Measurement of electrical conductivity to elucidate transport properties of RMs as a function of binary compositions of polar solvents and surfactant charge types

As it is well-known that the measurement of electrical conductivity of RMs is influenced by their microstructures, we intend to monitor the changes in conductance behaviour of “dry RMs” as a function of the polar solvent’s content, which is illustrated in Fig 3A and 3B.

The results show two different behaviors pertaining to the dependence of conductance on the composition of binary cosolvent in D_{12}DAB RMs. Aqueous RMs along with the systems with binary water-ACN content in the range of 90% to 60% (v/v) showed bell-shaped curve. Thus, a distinct increase in conductivity is evidenced with a broad maximum and followed by sharp decrease after passing through the maximum (Fig 3A). On the other hand, pure non-aqueous RMs (100% v/v of ACN) and RMs with binary water/ACN compositions in the range of 50% to 10% (v/v) showed a sharp increase in conductivity up to the phase separation (Fig 3B). The conductance of w/o RMs at lower volume fraction of water or at a state much below the percolation threshold can be explained on the basis of migration of statistically charged droplets

with charge fluctuation features [26]. An increase of the content of water or water-rich binary mixture increases the mobility of surfactant ions during the "fusion-fission" process, which tends to increase the electrical conductivity [27]. Herein, the addition of water or water-rich polar solvents (90% to 60% of water) into D_{12}DAB-formed RMs favours the charging process and tends to increase the electrical conductivity. On the other hand, the size of the RM droplets generally increases with more water-rich polar solvent solubilizing in RMs, which results in a slow migration of droplets under electric field and lowers the conductivity. These two antagonistic effects counteract with each other and result in a maximum conductivity with increasing water-rich polar solvent content in D_{12}DAB/Cy RMs [28].

On the other hand, the sharp rise in conductivity for non-aqueous and ACN-rich RMs is due to the following reasons. The solubilization of higher amount of ACN (50%, v/v) in the water pool may decrease the association interaction between water molecules and head groups of D_{12}DAB by weakening the polarity of water, and this results in the decrease of interfacial rigidity of droplets and benefits the formation of transient channels between the consecutive droplets. Moreover, the interdroplet attractive interactions become stronger with increasing concentration of ACN, and the droplets become more interconnected and easily form the transient channel for ions transfer with increasing polar solvent content, and thus the conductivity is increased sharply [29]. Thus, it can be summarized from the following results that conductance behaviour in D_{12}DAB RMs containing 100% to 60% water (ω_0=3.70-2.22) as polar phase governed by the counter-balancing effects of two mechanisms (i.e., "hopping" and "fusion-fission"); whereas charge migration mechanism through interconnected droplets played important role for 50% to water to 100% ACN based (ω_0=1.85-0) D_{12}DAB RMs. These results pointed out that a structural transition in D_{12}DAB RMs occurred at a particular composition of polar solvent, i.e., 50% of water (v/v) or ω_0 of 1.85.

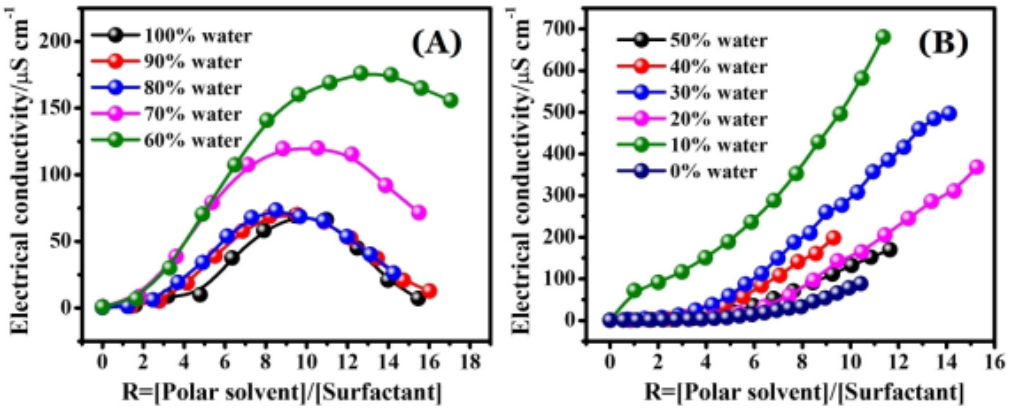

Figure 3. Electrical conductivity of D_{12}DAB/cyclohexane reverse micelles (RMs) composed of different binary compositions of polar solvents (water or ACN, v/v) as a function of molar ratio of polar solvent to surfactant (R) at 298 K, where (A) RMs with 100% water to 60% water, and (B) RMs with 50% water to 0% water. Herein, 10% water to 100% (v/v) water systems correspond to the water/surfactant molar ratio (ω_0) of 0.37 to 3.70.

In order to understand the influence of the interfacial charge of RMs on the structural transitions of aqueous to non-aqueous systems, similar conductance study was undertaken for AOT/Cy RMs. Surprisingly, the bell-shaped curve is obtained only for limited systems, e.g., pure aqueous and few water rich AOT RMs (90% and 80% v/v of water) (Fig S1, Appendix A). However, most of the binary RM systems along with pure non-aqueous one revealed a regular increase in conductivity and subsequently, percolation phenomena (Fig S1). Appearance of percolation in conductance in RM systems can be correlated with the transition from discrete droplet type to connected droplet type microstructures and also the increase of interdroplet interaction as well. According to Garcia-Rio et al. [30], electrical conductivity in an AOT-based microemulsion is due to the passage of cations through the transient channels formed between colliding droplets. This passage is facilitated by the formation of the certain local region of positive curvature in AOT surfactant film [31]. The fluidity of the interface and the attractive interactions among the aggregates are the most important factors that determine the exchange rate of the ions during the fusion processes [32], which leads to percolation. At this juncture, it is worth comparing the conductance phenomena in two RMs (cationic and anionic) at a similar polar phase composition. It can be observed from subsequent figures that in most of the systems, the conductance

values are found to be higher for D_{12}DAB RMs compared to AOT RMs. However, at or near equivalent binary polar phase compositions (50% and 60% of water), AOT RMs shows a distinct percolation phenomena with larger conductance values compared to D_{12}DAB RMs. These results clearly indicate the important role of surfactant charge types which mainly governs the interdroplet interaction within the RMs.

V.3.4 Molecular states of water in confined environment of RMs in presence of ACN by FTIR spectroscopy

Over the past decade, there was intense research to understand the details of water structure solubilized in the heterogeneous media. Thus, it is also necessary to study the states and properties of solubilized water in these formulated RM media and further to examine how the added ACN molecules change the microstructure of the aqueous RMs. Earlier, the states of dissolved water in aqueous microemulsions were intensively investigated and found to depend strongly on the content and the nature of the surfactant head groups [28,33–35]. Herein, the states of water in presence of ACN in D_{12}DAB RMs have been investigated by FTIR spectroscopy, which further resolved to the trapped water, bound water, and free water components by least-squares curve fitting on the basis of Gaussian peak shape. For the traditional aqueous RMs, the entrapped water has in general three distinct states: trapped, bound, and free or bulk-like water. The trapped water, with OH stretching vibration at ~3600 cm^{-1}, is defined as the water species dispersed among long hydrocarbon chains of surfactant molecules. It exists as monomers (or dimers) and has no hydrogen bonding interaction with its surroundings is expected. As the trapped water molecules are matrix-isolated dimers or monomeric in nature, they absorb in the high frequency region. The bound water molecules are hydrogen bonded with the polar headgroups of surfactants, which results in absorption in the low-frequency region of the IR spectrum and appears at ~3400 cm^{-1} [28,33–35]. In these RMs, ACN is also used as polar solvent for entrapment into RMs along with water. It was reported previously that water can bind with ACN molecules through the formation of OH–N bonds at the expense of O—H—O bonds [36]. Therefore, the water hydrogen bound to ACN in mixed RMs may also be appeared as bound water and is fitted together. Apart from these two types of water species, the free water molecules, occupying the cores of surfactant aggregates, have strong hydrogen bonds among themselves, that is, they have similar bulk water properties, which shift

the OH stretching band to a lower frequency at 3220 cm^{-1}. The OH stretching regions of D_{12}DAB RMs with 100, 60 and 10% added water are shown in Fig 4A-C, respectively. It can be seen that the data curve fits the experimental points quite well in all the cases. Similar fittings were performed for other compositions as well. The dependence of the area fractions for the three water species (trapped, bound, free water) as a function of the overall water content in presence of ACN in D_{12}DAB RMs is presented in Table S1 (Appendix A). Population of bound water is gradually increased on going from 100% to 50% water fraction at the expense of both bulk and trapped water and thereafter reversal of trend observed from 40% to 10% water fraction in D12DAB RMs.

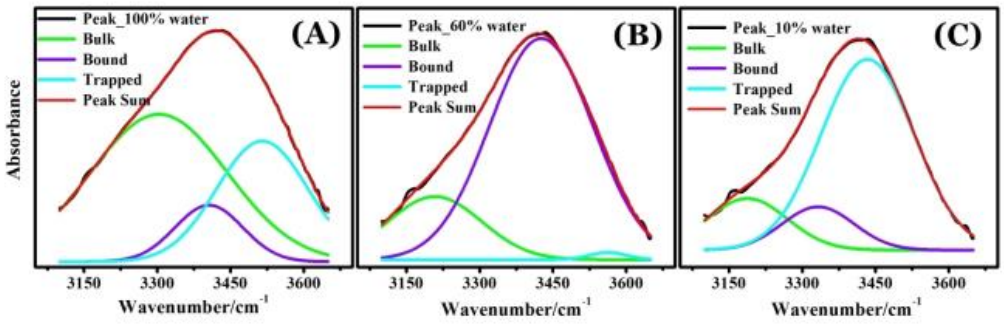

Figure 4. Representative FTIR spectra of OH band in D_{12}DAB/cyclohexane reverse micelles (RMs) composed of different binary compositions of polar solvents (water or ACN, v/v) at 298 K, where (A) RMs with 100% water (ω_0 = 3.70), (B) 60% water (ω_0 = 2.22), and (C) 10% water (ω_0 = 0.37).

Observing the various water states inside RMs, one can explain the results in terms of transition from ACN-rich RMs (10% to 50% water, v/v) to water-rich RMs (60% to 90% water, v/v) and subsequent formation of pure aqueous RMs (100% water, v/v). The fraction of bound water is gradually increased at the expense of bulk-like or free water, when 50% ACN-based RMs is reached from 10% ACN. In D_{12}DAB/Cy/ACN non-aqueous RMs, the counter ions become highly solvated after disruption of the intermolecular structure of ACN inside the confinement. As a result, the quaternary ammonium head groups of D_{12}DAB become available to interact, on increasing the water concentration in polar solvent mixture, and more and more bound water starts to form along with substantial amount of trapped water (10% water RMs, Fig 4C). The water molecules which are mainly located in the palisade layer are either mechanically trapped within the reverse micellar structure or thermodynamically bound to the ionic head groups of D_{12}DAB and ACN via hydration or intermolecular hydrogen bonding. It

is also observed that at very low water concentration (10%, v/v), water molecules mainly behave as the trapped water and with increasing concentration (20% to 50%, v/v), the trapped water fraction decreases and bound water fraction increases. On increasing the concentration, a reversal of trend occurs for bulk and bound water molecules in water-rich and aqueous RMs. This is obvious because, the water molecules began to enter the nano-pools once the bound water reached the saturation point. As a result, population of free water increases and reaches maximum in aqueous RMs (Fig 4A) at high water content.

V.3.5 Location and molecular states of ACN in D_{12}DAB and AOT RMs from FTIR measurement

In order to understand the location and H-bonded environment of ACN molecules in both aqueous D_{12}DAB and AOT/Cy RMs, the IR spectra in υ_{CN} region have been collected at different volume fraction of ACN in studied systems, which are shown in Fig S2A-B (SI). Red-shifted υ_{CN} is observed with increase in ACN concentration in both RMs, which is observed earlier for bulk water-ACN mixture [36]. However, it is worthwhile to mention that the υ_{CN} frequency is more red-shifted for AOT RMs compared to D_{12}DAB RMs at comparable composition of ACN (v/v) (Fig 5A-B), which indicates stronger interaction between ACN with negatively charged surfactant interface (herein, AOT) compared to positively charged interface (herein, D_{12}DAB). The nitrogen atom in ACN's CN group can interact either with another ACN molecule or with OH group of water [36] and polar head groups of surfactants. To identify the molecular states of ACN in confined environment of both D_{12}DAB and AOT RMs, we therefore considered fluctuations in the band frequency that occur differently (randomly) for individual members of the overall distribution and lead to Gaussian contributions to the band. The representative deconvoluted spectra in υ_{CN} region of D_{12}DAB and AOT RMs are represented in Fig S3A-B (SI). The deconvoluted lower frequency is termed as 'network or free' ACN, whereas the higher frequency band is termed as 'interfacial or bound' ACN [36,37]. The variations in the area fraction of both molecular states of ACN in D_{12}DAB and AOT RMs are shown in Fig S3C-D (SI). It is evident from the figures that in D_{12}DAB RMs, the 'network and free' ACN increases at the expense of 'interfacial or bound' ACN with increasing concentration of ACN in RMs, which was earlier observed for bulk water-ACN mixture too.[36] But,

the ‘interfacial or bound’ ACN increases with increasing ACN concentration for AOT RMs, due to their favorable interaction with negatively charged interface. However, after comparing the result for two RMs, we observed larger fraction of ‘bound’ and lower fraction of ‘free’ ACN in AOT RMs compared to D_{12}DAB RMs at higher concentration of ACN (50% to 100%, v/v) (Fig 5C-D). These observations certainly proves that ACN molecules are more prone to sit near the interface of AOT RMs compared to D_{12}DAB, which is well supported by the theoretical calculations (described in subsequent section).

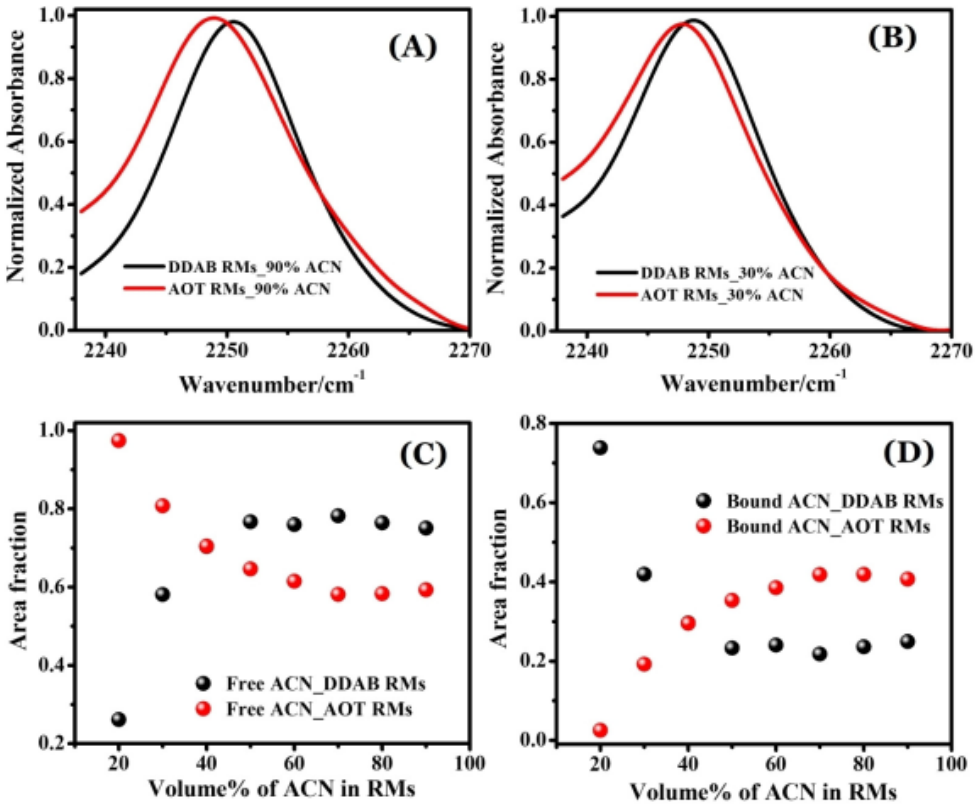

Figure 5. FTIR spectra in υ_{CN} region of ACN molecules in D_{12}DAB and AOT/cyclohexane reverse micelles (RMs) composed of different binary compositions of polar solvents (ACN or water, v/v) at 298 K, where (A) RMs with 90% ACN, and (B) 30% ACN. Gaussian deconvoluted area fraction of various ACN states in RMs, where (C) ‘free’ and (D) ‘bound’ ACN molecules.

V.3.6 Characteristics of nano-water pool in D_{12}DAB-RMs in presence of ACN by UV-Vis spectroscopy

In order to further explore the effect of ACN on the microstructure of the aqueous RMs to identify its actual locations, it is important to confirm the formation of nano-pools in these systems. For this purpose, a metal salt, $CoCl_2$ was chosen, which is insoluble in Cy, but soluble in D_{12}DAB/Cy mixture and in bulk water or ACN. Fig 6A-D represent the UV/Vis absorption spectra of $CoCl_2$ solubilized in RMs as a function of added content of polar phase (100%, 50% and 10% v/v of water and 100% v/v of ACN). The absorbance of Co^{II} in D_{12}DAB/Cy RMs showed a broad band at 525–725 nm region comprised of a few convoluted peaks similar to earlier reports [38–40]. Interestingly, for aqueous RMs, an extra band appears at near 510 nm, which is a characteristic of the absorbance of Co^{II} in aqueous medium. The absorbance of the 510 nm band increases with a subsequent decrease in the absorbance of the lower energy bands with gradual addition of water in aqueous RMs. These results indicate the formation of bulk water pools within the D_{12}DAB/Cy/water (100% v/v) RMs as is expected in case of w/o microemulsions. This observation indicates that $CoCl_2$ is solubilized in an environment that is similar to bulk water. The formation of nano-pools is further confirmed if one compares the absorbance of Co^{II} in non-aqueous RMs with that of 100% of ACN (v/v) at constant $CoCl_2$ concentration. Unlike the absorbance of Co^{II} in aqueous RMs, the absorbance of Co^{II} for the non-aqueous systems shows no additional band at 510 nm. Even in ACN-rich RMs (10% water, v/v), the band at 510 nm was found to be absent. These changes in the spectral behaviour of Co^{II} are because Co^{II} is initially solvated within D_{12}DAB/Cy solution with no water, thus predominantly existing as tetracoordinated species [40]. When water content in mixed binary solvent based-RMs increases, it exists in a dispersed form associated with the surfactant monomers within the solution through H-bonding. Once RM system reaches a threshold limit (i.e., 100% v/v of water RMs), water starts to form water pools with the help of appropriately aggregated D_{12}DAB and subsequently accumulates in the core of thus formed RMs where the majority of water is now present in its free form with properties similar to those of bulk water.

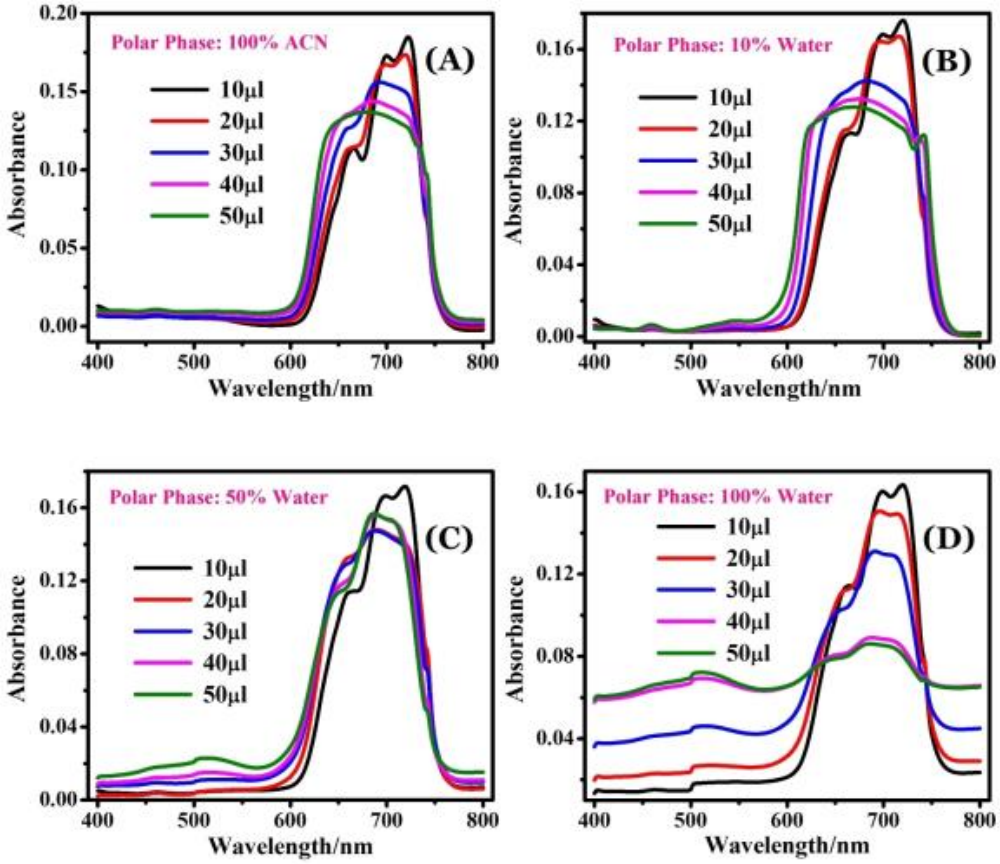

Figure 6. UV/Vis absorption spectra of $CoCl_2$ dissolved in D_{12}DAB/cyclohexane reverse micelles (RMs) after gradual addition of polar solvents at different binary compositions (v/v) at 298 K, where (A) RMs with 100% ACN or 0% water, (B) 10% water (ω_0 = 0.37), (C) 50% water (ω_0 = 1.85), and (D) 100% water (ω_0 = 3.70).

V.3.7 Evidence of H-bonding environment from the temperature-dependent droplet size measurement using DLS for D_{12}DAB/Cy RMs

Finally, to examine the H-bonding efficiency in these systems and their response towards temperature, we measured temperature-induced droplet sizes of the individual RM systems in the temperature range of 298–313 K. While heating, all the systems were found to remain transparent in the whole temperature range studied. As shown in Fig 7A-C, the size of the droplets in aqueous RMs and ACN-rich RMs (30% and 10% water, v/v) decreases with temperature.

In general, increase in the temperature leads to swelling of the D_{12}DAB tails by the solvent and hence a decrease in the spontaneous curvature of the D_{12}DAB monolayer and this leads to the formation of smaller droplets [41]. Interestingly, the change in

droplet size as a function of temperatures is found to be prominent for aqueous RMs, whereas no noticeable changes are observed for ACN-rich RMs. In order to examine the thermal stability more accurately, we illustrate the change in droplet size from 298 to 313 K as a function of different composition of binary solvent in RMs (Fig 7D). It is clear from the plot that the temperature-sensitivity is gradually reduced on going from aqueous RMs to non-aqueous RMs. This dependence seems obvious if one considers the extent of H-bonding ability in these systems and is attributed to a disruption of H-bonding, between the water and the polar head group of $D_{12}DAB$ molecule at high temperature [42]. As the system proceeds towards the ACN-rich RMs, the lack of H-bonding ability of ACN with surfactant actually provides more temperature insensitivity to the formulated systems.

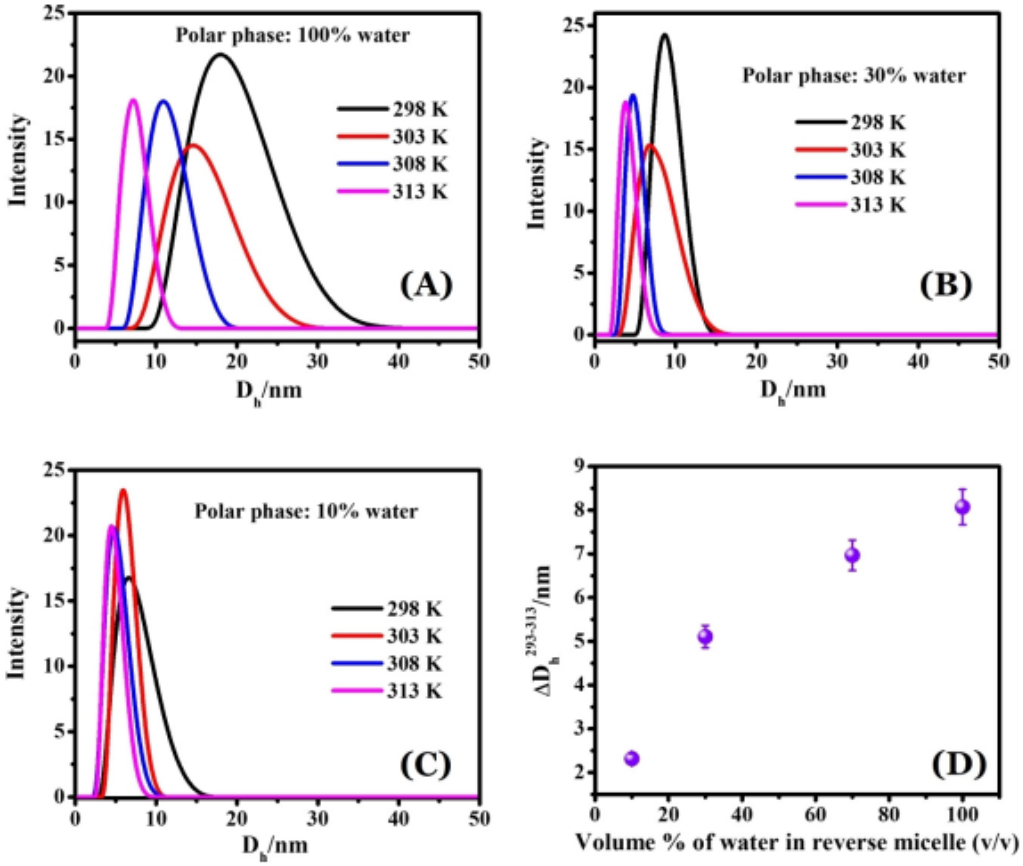

Figure 7. Size distribution of $D_{12}DAB$/cyclohexane reverse micellar (RMs) droplets as a function of temperature composed of different binary compositions of polar solvents (water or ACN, v/v), where (A) RMs with 100% water (ω_0 = 3.70), (B) 30% water (ω_0 = 1.11), and (C) 10% water (ω_0 = 0.37). (D) The change in droplet size from 298 to 313 K ($\Delta D_h^{298-313}$) as a function of volume % of water (0% to 100%), which is equivalent to ω_0 of 0.37 to 3.70 in RMs.

V.3.8 Microenvironment of D_{12}DAB/Cy RMs in presence of ACN using 7-hydroxycoumarin

In continuation of our interest in the microenvironmental characterization of aqueous and non-aqueous RMs, we herein report the absorption characteristics of the dye 7-hydroxycoumarin (7HC) (Fig 8A) in mixed compositions of bulk polar solvent and RMs at similar binary solvent compositions. 7HC is widely used as a polarity indicator in various RM media [43,44]. 7HC is insoluble in hydrocarbon and sparingly soluble in water [44]. It is soluble in hydrocarbons in presence of D_{12}DAB. The dye solution added to the D_{12}DAB/Cy/polar solvent is expected to reside at the surfactant monolayer formed between the two immiscible phases. The observed physicochemical changes should refer to the properties of the interfacial region of RMs. The absorption profiles of 7HC in bulk solvents and RMs are illustrated in FIG 8B. It is clearly seen that the absorption maxima of these RMs are blue-shifted compared to the bulk solvents, which is observed earlier [45]. This observation supports the lower static polarity of the reverse micellar core compared to bulk solvents. It is interesting to note that with increasing concentration of ACN in RMs, the absorbance decreases with slight blue-shift. This is possible if ACN enter into the RM interface of D_{12}DAB by ion-dipole interaction forming a sparse interface which is less susceptible to accommodate 7HC molecule. Thus 7HC preferably resides on the pseudo RM phase and hence the rate of change in absorbance decreases [44]. The blue shift in absorption maximum with increase in ACN concentration is due to the decrease in the local polarity around the 7HC in RM medium. 7HC consists of an electron donating group (hydroxyl group) and an electron withdrawing aromatic system. The direction of the excited state charge flow is from the hydroxyl group to the carbonyl group across the aromatic ring and the twisted intra-molecular charge transfer process gives an excited state with a large dipole which is stabilized in more polar environments. The blue-shifted absorption maximum of 7HC from polar protic solvent (water) to aprotic solvent (ACN) entrapped in RMs is due to the changes in its excited state dipole moment. The hydrophilic nano-pool region present in the reverse micellar form is significantly reduced in polarity when more and more ACN is entrapped due to their lack of H-bonding ability. The efficient partitioning of 7HC in presence of ACN from nano water pool to the interfacial region may be the possible reason for the blue shift in the absorption maximum as is shown in FIG 8B.

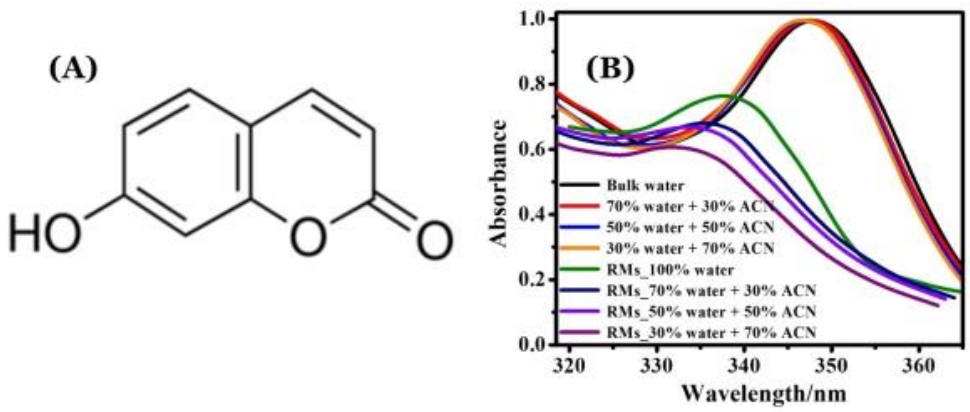

Figure 8. (A) Chemical structure of 7-hydroxycoumarin (7HC) and (B) Absorption characteristics of 7HC in bulk compositions of polar solvents (water or ACN, v/v) and in D_{12}DAB/cyclohexane reverse micelles (RMs) as a function of binary compositions of water or ACN at 298 K.

V.3.9 Quantum chemical calculation for determination of binding energy responsible for the interactions between surfactants and polar solvents

Finally, we undertook ab initio calculations to have insights on the molecular level interaction between cationic (D_{12}DAB) as well as anionic (AOT) surfactants and entrapped polar solvents (water and ACN). In the RM core, primary stabilization forces come from the interactions of cationic or anionic head groups of D_{12}DAB or AOT, respectively with water or ACN or both water and ACN, when ACN molecules are present with water. Accordingly, we have optimized the structures of D12DAB or AOT-water, D12DAB or AOT-ACN and D_{12}DAB or AOT-water-CAN complexes and obtained the energy of interactions from single point energy calculation. To represent the energy of interactions accurately, single point energy of the optimized structure of each constituent is subtracted from the energy of whole complex. It is also worth mentioning here that during the structural optimizations, we modeled both D_{12}DAB and AOT by cutting their hydrocarbon chain lengths without changing the conformation of head groups. Since the distant part of surfactant tails has minor influence on water or ACN-head group interactions, this approximation would have little influence on the overall results. Also, in order to mimic our experimental conditions, we took either two molecules of water or ACN or one molecule of water with one molecule of ACN with AOT or D_{12}DAB by keeping total number of molecules same in each complex. The optimized structures of D_{12}DAB, AOT and six complexes along with their stabilization energies (kcal/mol) are illustrated in Fig 9 and 10(A-D).

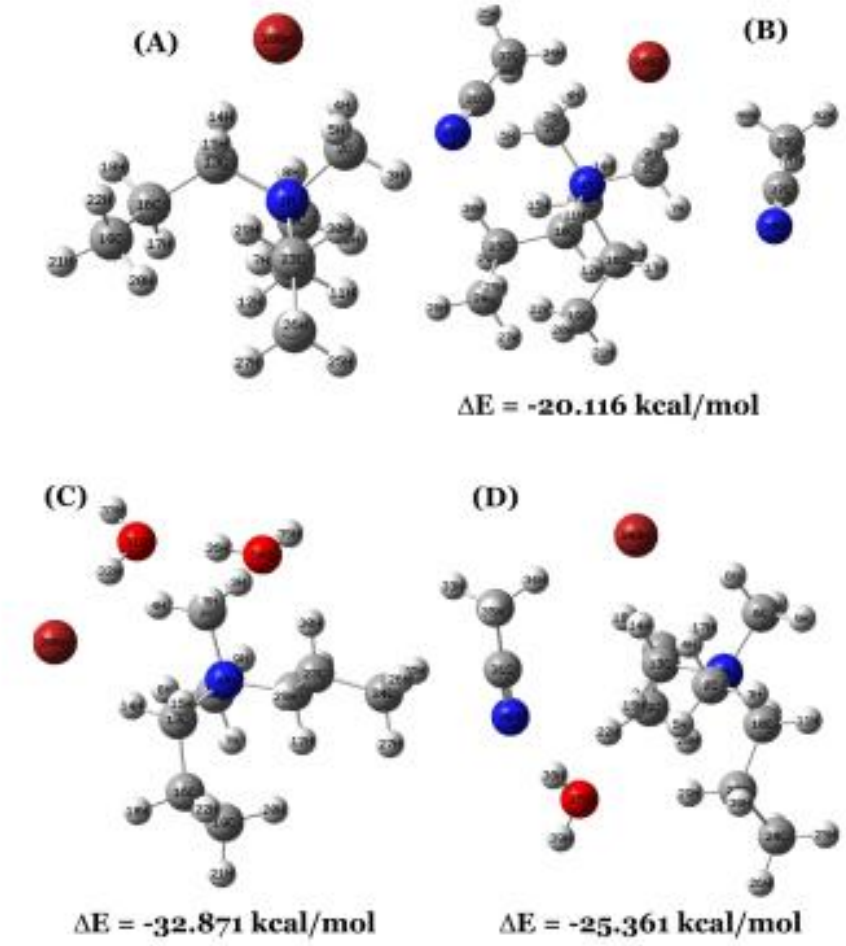

Figure 9. Minimum energy structures of (A) D_{12}DAB head group, (B) D_{12}DAB head group + ACN, (C) D_{12}DAB head group + water, and (D) D_{12}DAB head group + water + ACN. Interaction energies (DE) are obtained by subtracting the energies of the individual optimized structures of each constituent from the energy of the optimized structure of the whole complex.

The relatively large ΔE value was obtained (ΔE= - 32.871 kcal/mol) for D_{12}DAB-water complex and followed the order: D_{12}DAB-ACN < D12DAB-ACN-water < D_{12}DAB-water. This indicates the presence of ACN reduced the stability of D_{12}DAB-water complex. As we have stated earlier that ACN interacts with D_{12}DAB by weak dipole-dipole interaction whereas strong interaction occurs in case of D_{12}DAB and water molecules. Thus, ACN at high concentrations gradually decreased the interaction between D_{12}DAB and water in aqueous RMs and results in the smaller droplet size, larger number of droplets along with higher conductivity, reduced population of bulk-

water, movement of optical probe towards outer surface of polar nano-pool and even non-appearance of nano-pool at its higher volume fraction. Similar results also obtained for AOT systems and the corresponding stabilization energies are given in respective figures (Fig 10A-D). It is also worth mentioning here that the stabilization energies for surfactant-ACN or ACN-water or water complexes are found to be higher for anionic AOT systems compared to D_{12}DAB systems.

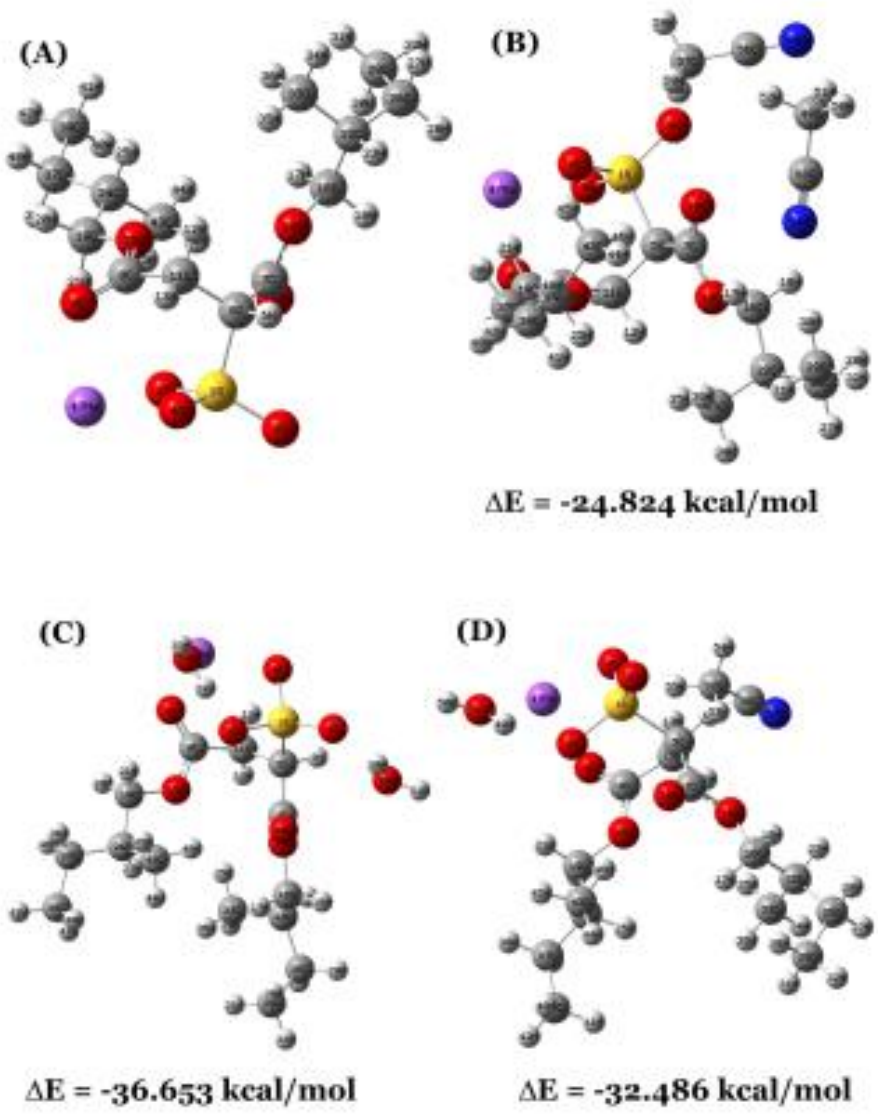

Figure 10. Minimum energy structures of (A) AOT head group, (B) AOT head group + ACN, (C) AOT head group + water, and (D) AOT head group + water + ACN.

V.3.10 Molecular electrostatic potential of different constituents of cationic and anionic RMs

Further, electrostatic potential (ESP) of each isolated molecule was computed at HF/6-31G level of theory. Fig S4 (Appendix A) demonstrates a conventional color pattern of ESP in which the regions with the strongest negative electrostatic potential are coloured in red and those with the strongest positive electrostatic potential in blue. The regions with zero potential are represented in green. The electrostatic potential increases in the following order: red < orange < yellow < green < blue. The negative electrostatic potential corresponds to an attraction of the proton by the aggregate electron density in the molecule (shades of red), while the positive electrostatic potential corresponds to the repulsion of the proton by the atomic nuclei (shades of blue). The ESP map indicates that the negative electrostatic potential regions are mainly found over the oxygen atom of water, nitrogen atoms of ACN, and to the quaternary nitrogen and bromine of D_{12}DAB, these regions being possible active sites for electrophilic attack. The positive regions are localized around all the hydrogen atoms, these being the most probable sites for nucleophilic attack [46]. As can be seen from Figure S4, the maximum value of charge separation is attributed to the modeled AOT, followed by D_{12}DAB and water molecules, and the lowest corresponding value belongs to the ACN. Consequently, it can be predicted that the strongest interactions are ascribed to the water/AOT complex, and the weakest interactions are attributed to the ACN/D_{12}DAB complex. Similar kind of observation was also reported earlier in order to show differential interaction between a surfactant (TX-100) and molecular solvents such as methanol, ethanol, 1-propanol, and water [47].

V.3.11 Theoretical predictions of vibrational signatures for D_{12}DAB-water-ACN complexes

The IR spectral range of bending and stretching OH vibrations at around 1500 and 3600 – 4000 cm^{-1}, respectively for water molecules and stretching vibrations of C≡N in ACN molecules are highly sensitive to environmental changes. Fig S5A-F (Appendix A) show the full range of the calculated FT-IR spectra of water, ACN, D_{12}DAB molecules and their corresponding complexes in gas phase. The major peak positions (mentioned above) of water and ACN molecules were assigned based on the animated vibrations of bond from the calculations. The changes in assigned band frequency of water and ACN

in different complexes (such as, water ACN, D_{12}DAB-water, D_{12}DAB-ACN, and D_{12}DAB-water-ACN) is depicted in Fig S6 (Appendix A). Red-shifted vibration frequencies of the bending and stretching OH and C≡N vibrations in complexes compare to pure molecules suggest the preferential binding of water and ACN with D_{12}DAB through H-bonding interaction. However, both symmetric and asymmetric as well as bending vibrations of water shows maximum shifts to the lower wavenumber region in vibrational band (Fig S6), which clearly indicates that the D_{12}DAB-water complex is energetically favourable than D_{12}DAB-ACN or D_{12}DAB-water-ACN complexes.

V.4. Conclusion

In this work, we have formulated D_{12}DAB or AOT/Cy RMs based on different volume fraction of polar solvents, e. g., water and ACN. Our primary objective is to show that how the stability, microstructures (sizes, transport properties and states of encapsulated polar solvent) and H-bonding environments of RMs would be modified along with the change in the microenvironment from aqueous to non-aqueous milieu and also to establish the possible influence of surfactant charges on this transitions. Since only a few researchers who had worked in this field, mainly concentrated on the formulation and characterization of either pure aqueous RMs or ACN-based non-aqueous RMs [1,48], we have undertaken this study, where a comparative results along with microstructural characteristics of aqueous (water) and non-aqueous (ACN) RMs along with several water-rich and ACN-rich RMs has been discussed. Maximum solubilization capacity of particular binary compositions of polar solvent in RMs achieved for 50% and 20% of entrapped ACN in mixed polar solvent for D_{12}DAB-and AOT-RMs, respectively. Similarly, two different types of conductance mechanisms govern the microstructural changes of aqueous, water-rich and non aqueous, ACN-rich RMs for AOT and D_{12}DAB systems. Droplet size has been found to be gradually decreased as one go from aqueous to non-aqueous D_{12}DAB/Cy RMs. Different types of nano-confined water (free, bound and trapped) and ACN (free and bound) are found, the fraction of which vary as one go from water-rich compositions to ACN-rich compositions. AOT-RMs produced higher fraction of bound ACN compared to D_{12}DAB-RMs along with the more red-shifted υ_{CN} vibrational band, which confirmed localization of ACN near to AOT compared to D_{12}DAB. This observation is further

clarified from the observed higher stabilization energies for AOT-ACN complexes than that for D_{12}DAB complexes. Molecular probe 7HC confirmed localization of ACN near to the surfactant interface of D_{12}DAB-RMs from absorbance profiles. Further, from temperature-independent droplet size distribution of pure non-aqueous along with ACN-rich D_{12}DAB/Cy RMs proved absence of H-bonding environment. Bulk nano-pool of polar solvent found to be progressively disappeared as we moved from aqueous to non-aqueous RMs. Finally, ab initio calculations confirmed the occurrence of weaker interaction between surfactant and polar solvent in presence of ACN. It is believed that the present study would give an overview of the mechanism of formation of aqueous and non-aqueous ACN-based RMs along with the microstructural transformations. This result may pave the way for the application of the non-aqueous RMs as potential nanoreactors, e. g., in nanoparticles synthesis, via controlling the inter micellar interactions and thus tuning the size and morphologies of the nanoparticles [48–50].

References are provided in BIBLIOGRAPHY under “References for Chapter V” (Page 141-143)